Ingénierie des Systèmes d'Information
Vol. 30, No. 2, February, 2025, pp. 367-373
Journal homepage: http://iieta.org/journals/isi

# Classification and Analysis of Parkinson's Disease Based on Gabor and Wavelet Filters

Vijay Khare[1*], Ramit Kumar[2]

[1] Department of Electronics and Communication Engineering, Jaypee Institute of Information and Technology, Noida 201309, India
[2] Department of Information Technology, Netaji Subhas University of Technology University, Delhi 110078, India

Corresponding Author Email: vijay.khare@mail.jiit.ac.in



https://doi.org/10.18280/isi.300208

**Received:** 30 September 2024
**Revised:** 5 January 2025
**Accepted:** 14 January 2025
**Available online:** 27 February 2025

***Keywords:***
*amplitude of low frequency fluctuations (ALFF), fractional ALFF (fALFF), regional homogeneity (ReHo) and functional connectivity (FC), Parkinson's disease (PD)*

**ABSTRACT**

Parkinson's disease (PD) is a neuro-degenerative disease, which develops with age and has symptoms such as tremors, amnesia, and hindered movements. In this paper, the analysis of functional Magnetic resonance imaging (fMRI) data is performed to differentiate activity of the brain between PD affected person and a normal person. The amplitude of low frequency fluctuations (ALFF), fractional ALFF (fALFF), regional homogeneity (ReHo) and functional connectivity features are used for the analysis. Further, Gabor filters and wavelet decomposition are applied on feature images to improve classification accuracy. Three different classifiers, namely Naïve Based, Logistic Regression SMO and Decision Stump have been used for classification. The Decision Stump shows 65% classification accuracy with Gabor filter and 90% classification accuracy with wavelet transform analysis. This shows the wavelet transform method is more suitable over Gabor filter in the classification for fMRI data of PD.

## 1. INTRODUCTION

Parkinson's disease (PD) is a chronicle movement disorder that gets worse with age and affects millions of people [1]. PD is symptomatically characterized by lack of coordination, memory loss and bradykinesia because of the breakdown of vital nerve cells in the brain. Nerve cells are responsible for producing dopamine, the essential chemical for proper brain functioning [2].

In literature, several diagnoses have been proposed for PD, but the diagnosis still relies on clinical symptoms [3]. However, the early stage symptoms are not sufficient to diagnose PD. Various Neuro-imaging methods are SPECT-imaging, MRI and PET to diagnose PD have shown promising results [3, 4]. But these methods are still not conclusive since they do not provide characteristic features of functional connectivity [5, 6]. These methods come with notable limitations. SPECT imaging, though useful, provides lower spatial resolution compared to other neuroimaging techniques, which can hinder precise localization of affected regions. MRI primarily captures structural changes, which may not reveal the early functional abnormalities critical for PD diagnosis. PET imaging, while offering high sensitivity, is invasive, requires the use of radioactive tracers, and involves significant cost, making it less accessible for routine diagnostics. These shortcomings underscore the need for a more effective approach, such as fMRI, which is non-invasive, provides high-resolution functional and structural imaging, and captures real-time neuronal activity, offering greater potential for early detection of Parkinson's disease. But by performing fMRI analysis, functional connectivity of neurons is explored for the diagnosis of PD.

Analysis of fMRI data encompasses evaluation of activity at specific regions of interest. Numerous strategies for extraction of activity data are found in the literature. Decomposition of fMRI time series data using a wavelet is one such scheme discussed in the studies [7, 8]. In another study, the fMRI data is filtered using wavelets and correlation between resulting signals giving functionally connected brain topography [9]. Gabor wavelet pyramid was used by Kay to measure voxel activity patterns [10]. In this paper, analysis of fMRI data is done to differentiate between PD patients and healthy subjects. There are few advantages using fMRI data. fMRI is a non-invasive technique, eliminating the need for surgical procedures or radiation exposure. fMRI provides high-resolution images of brain structure and function, enabling precise localization of affected areas. fMRI measures brain activity, providing insights into functional changes associated with Parkinson's disease.

The rest of the paper is organized as follows: The analysis steps, features extracted and region of interest are explained in Section 2. In Section 3, Gabor filter, wavelet analysis and classification method are discussed followed by results in Section 4. The paper is concluded in Section 5.

## 2. RESEARCH METHODS

The flow chart for fMRI Data analytics using Gabor and wavelet filters of PD patients is given in Figure 1.

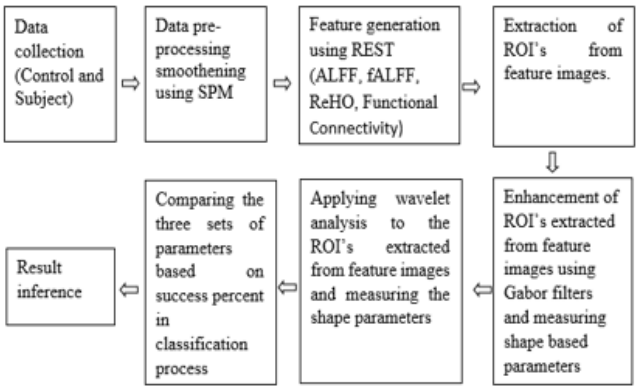


**Figure 1.** Flowchart of data analysis

The data set was collected from the Parkinson's progression markers initiative (PPMI) [11]. The data set comprised 10 healthy patients including 6 males and 4 females, and 10 PD patients, including 5 males and 5 females for resting state fMRI. The scan amounts for a period of 504 seconds with a TR of 2.4 seconds for each patient. The age group of subjects was 40-75 years.

For the analysis of PPMI data set, the following software platforms are used: MATLAB 7.10.0, SPM8, NIFTII for Image View, and REST. There are advantages for these tools:

**MATLAB 7.10.0:**

1. High-level programming language: Easy to learn and use, with extensive toolboxes and libraries.
2. Rapid prototyping: Quick development and testing of algorithms and models.
3. Large community: Access to a vast user community and resources.

**SPM8 (Statistical Parametric Mapping):**

1. Advanced image analysis: SPM8 provides a wide range of tools for image processing, statistical analysis, and visualization.
2. Neuroimaging expertise: Developed by neuroimaging experts, ensuring accuracy and relevance.
3. Integration with MATLAB: Seamless integration with MATLAB, leveraging its strengths.

**NIfTI (Neuroimaging Informatics Technology Initiative):**

1. Standardized format: NIfTI provides a standardized format for neuroimaging data, ensuring compatibility and exchangeability.
2. Easy data sharing: Facilitates collaboration and data sharing among researchers.
3. Wide adoption: Widely adopted in the neuroimaging community, ensuring compatibility with various tools.

**REST (RESTing-state fMRI analysis toolkit):**

1. Specialized toolkit: REST is specifically designed for resting-state fMRI analysis, providing tailored tools and methods.
2. Efficient analysis: REST offers efficient and automated analysis pipelines for large datasets.
3. Advanced metrics: Calculates advanced metrics, such as functional connectivity and network measures.

The selection of MATLAB 7.10.0, SPM8, NIfTI, and REST was driven by their specialized functionalities and widespread use in neuroimaging research. MATLAB offers a versatile programming environment with extensive libraries for rapid data processing and algorithm development. SPM8, integrated with MATLAB, is a robust tool for statistical and spatial analysis of neuroimaging data, designed by experts to ensure precision and reliability. NIfTI ensures data standardization and compatibility across platforms, enabling seamless sharing and collaboration. REST, tailored for resting-state fMRI analysis, provides efficient pipelines for advanced connectivity and network metrics. Together, these tools form a comprehensive framework for accurate and efficient analysis of the PPMI dataset.

### 2.1 Features extraction

The following features are used to analyze the PD patients and normal persons:

- **Amplitude of Low Frequency Fluctuations (ALFF):** The activity of the brain in the rest state is reflected by low frequency oscillations. The ALFF feature is the collective power contained in the low frequency band of 0.01Hz to 0.08 Hz. It helps to perceive the abnormally behaving regions in the rest state of the brain. **Physiological significance:** ALFF reflects spontaneous neural activity by measuring the amplitude of low-frequency oscillations, which indicates localized brain activity in resting-state conditions.
- **Fractional ALFF (fALFF):** The ALFF feature depends on the physiological noise. A ratio of the total power in the 0.01Hz to 0.08 Hz frequency band of to the total power in the 0 Hz to 0.25 Hz frequency band is obtained, so as to immunize ALFF from noise. This new measure is called fALFF feature [12]. **Physiological significance:** fALFF is a normalized measure of ALFF that reduces noise effects, highlighting physiologically relevant low-frequency oscillations and improving sensitivity to brain abnormalities.
- **Regional Homogeneity (ReHo):** The ReHo feature relates the synchronization in time series of voxels of fMRI and their nearest neighbor's. The Kendall's coefficient of concordance (KCC) is determined for the clusters of 27 voxels on the pre-processed fMRI images [13, 14]. **Physiological significance:** ReHo captures the synchronization of neural activity in adjacent voxels, reflecting localized functional coherence and abnormalities in regional connectivity.
- **Functional Connectivity:** It identifies the network of brain regions that show spontaneous co-activation. The functional connectivity of a region of interest (ROI) can be evaluated by measuring the time averaged course of ROI and by determining its correlation with time series of various regions. **Physiological significance:** It identifies coordinated activity across different brain regions, indicating the integration and communication within neural networks, which is crucial for understanding disrupted connectivity in PD patients.

A Gabor filter is used for texture analysis in image processing, an attempt to identify objects from obscure backgrounds. Its impulse response is defined by a 2D- plane sinusoidal wave multiplied by a Gabor envelope function [15].

$$g(x, y; \lambda, \theta, \psi, \sigma, \gamma) = exp\left(-\frac{x'^2 + \gamma'^2 y^2}{2\sigma^2}\right) exp\left(i\left(2\pi\frac{x'}{\lambda} + \psi\right)\right)$$

The real part of impulse response of Gabor filter is used for analysis and is given below:

$$x' = x\cos\theta + y\sin\theta\,, y' = -x\sin\theta + y\cos\theta$$

- σ: The standard deviation of the Gaussian envelope and controls the spatial extent of the filter. Larger values of σ result in a broader filter, capturing more global features, while smaller values focus on finer, localized details. In our study, σ is related to the bandwidth (b) and wavelength (λ) to balance spatial and frequency resolution.
- ψ: The phase offset determines the symmetry of the filter. A phase offset of 0 creates a symmetric filter (cosine-like), while π/2 produces an antisymmetric filter (sine-like). The values are chosen based on the dominant structural features in the region of interest (ROI).
- γ: The aspect ratio defines the ratio of the Gaussian envelope along the x- and y-axes. Smaller values elongate the filter, making it more sensitive to edge-like structures, while values closer to 1 produce circularly symmetric filters. For our analysis, γ=0.5 is selected to account for anisotropic structures.
- λ: The wavelength controls the scale of the sinusoidal wave, determining the frequency sensitivity of the filter. By analyzing the average diameter of the ROI, appropriate scales are selected as {0.8 * average diameter, average diameter, 1.2 * average diameter}.
- θ: The orientation defines the angle of the sinusoidal wave, allowing the detection of features at specific directions. In this study, orientations are set as π/6, π/4, π/3, π/2, 2π/3, and 3π/4 to comprehensively capture patterns in multiple directions.

σ is related to bandwidth ($b$) and wavelength (λ) of Gabor filters as:

$$\frac{\sigma}{\lambda} = \frac{1}{\pi}\sqrt{\frac{ln\,2\,\sigma}{2\lambda}} = \frac{1}{\pi}\sqrt{\frac{ln\,2}{2}}\frac{\{2^b+1\}\{2^b+1\}}{\{2^b-1\}\{2^b-1\}}$$

In analysis, bandwidth ($b$) =1, aspect ratio (γ) =0.5 and phase shift calculated after analyzing the average diameter of the region of interest as {0.8*average diameter, average diameter, 1.2*average diameter}. The total permutations of wavelength and orientations give us 18 Gabor filters as shown in Figure 2 [16]. These parameters are carefully selected to balance precision, scale, and orientation sensitivity for effective texture analysis in image processing.

The filtered images are normalized within [-1, 1] range [17, 18]. The threshold is calculated by the equitation given below:

Threshold = Mean – 0.5 × Standard Deviation

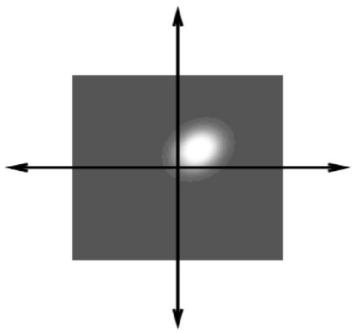

**Figure 2.** Gabor filter in the frequency domain

It is a modified form of Niblack's method. Niblack's method uses mean and standard deviation of pixels in a windowed area of image to calculate local threshold and segments a single image, while in the proposed method, mean and standard deviation are computed over many images.

### 2.2 Wavelet Analysis

Wavelets are primarily used to measure energy of certain frequencies of the signal in different intervals of time. The range of frequencies can be varied as per size of the time interval considered and thus give wavelet analysis resolution in both frequency and time.as shown in Figure 3.

In this proposed work, the Haar wavelet is used for image decomposition. The Haar wavelet is chosen due to its simplicity, computational efficiency, and effectiveness in capturing local features, such as edges and discontinuities, within the fMRI images. Its step-like function allows for rapid calculations, making it ideal for processing large datasets. Additionally, the Haar wavelet offers good data compression by producing sparse coefficients while retaining significant information, which is essential for efficient feature extraction.

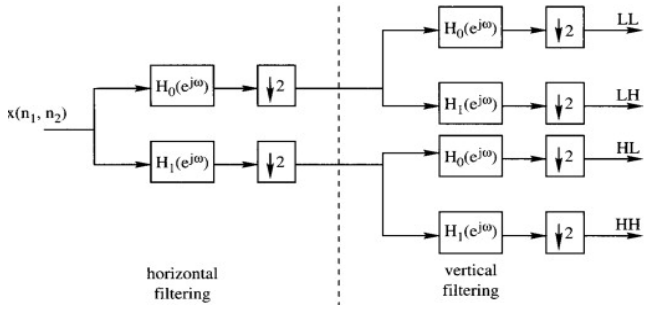


**Figure 3.** Wavelet filter decomposition

In a 2D image, the transformation is applied successively over rows and columns of the image. In MATLAB, the function 'wavedec2' finds the wavelet transform of an image using 'non-standard decomposition' for desired levels of decomposition and for specified mother wavelet.

The mother wavelet used is 'HAAR wavelet' [19]. Its mother wavelet function ψ(t) can be described as:

$$\varphi(t) = \begin{cases} 1 & 0 \le t < \frac{1}{2} \\ -1 & \frac{1}{2} \le t < 1 \\ 0 & \text{otherwise} \end{cases}$$

The scaling function ψ(t) is represented as

$$\Phi(t) = \begin{cases} 1 & 0 \le t < 1 \\ 0 & \text{otherwise} \end{cases}$$

In this work, the wavelet coefficients till decomposition of level 4 are obtained. The coefficients thus obtained are used to reconstruct images using MATLAB function 'wrcoef2' for level 4 decomposition to calculate the threshold parameters.

Also, reconstruction of an image at level 3 decomposition is done to provide a smoothed feature image, to which the threshold is applied.

### 2.3 Classification methods

The classifiers used in the study are Naïve Bayes, Logistic

Regression, SVM based on Sequential Minimal Optimization (SMO), and Decision Stump. These classifiers were chosen based on their distinct working principles and suitability for the classification task. The models were validated by a 10-fold cross-validation scheme, with the classification operations carried out using the WEKA software. A total of 504 attributes were generated to classify between healthy individuals and PD patients [20, 21].

**1. Naïve Bayes Classifier**

The Naïve Bayes classifier is based on Bayes' theorem, assuming that the features are conditionally independent. It calculates the probability of each class given the feature values and selects the class with the highest probability. This model is particularly useful when dealing with large datasets with independent features and works well for problems with categorical data. However, its assumption of feature independence may not always hold in complex datasets.

**2. Logistic Regression Classifier**

Logistic Regression is a statistical model used for binary classification tasks. It models the probability of a class as a logistic function of the input features. Logistic regression is widely used in scenarios where the relationship between the independent variables and the dependent variable is expected to be linear. It is effective when the classes are linearly separable and is interpretable, making it a good choice for many classification problems in health and social sciences.

**3. SVM based on Sequential Minimal Optimization (SMO)**

Support Vector Machine (SVM) is a powerful classifier that separates classes using a hyperplane in a high-dimensional space. The Sequential Minimal Optimization (SMO) is an optimization algorithm used for training SVMs. It is particularly efficient for large datasets and works well with both linear and non-linear problems using different kernel functions. SVM is effective when there is a clear margin of separation between classes, and its performance can be improved by choosing appropriate kernels and tuning hyperparameters.

**4. Decision Stump Classifier**

A Decision Stump is a simple machine learning model that combines the benefits of decision trees and stumps. Here's how it works:

- **Root Node:** The dataset is fed into the root node.
- **Feature Selection:** The algorithm selects the best feature (attribute) to split the data.
- **Threshold:** A threshold value is chosen for the selected feature.
- **Left Child:** Samples with values below the threshold go to the left child node.
- **Right Child:** Samples with values above the threshold go to the right child node.
- **Class Label:** Each child node is assigned a class label (prediction).

The algorithm iteratively selects the best feature and threshold to split the data. The process continues until a stopping criterion is met (e.g., maximum depth or minimum samples per node). The final prediction is made by combining the class labels from the child nodes. The Decision Stump classifier is suitable for simple datasets or as a weak learner in ensemble models like AdaBoost.

### 2.4 Computational steps

**1. Image Standardization and Elimination of Deviations**

The images obtained from PPMI are classified as PD patients or normal individuals. The SPM8 tool is used in image processing to standardize the scans and eliminate any deviations. This step is crucial to ensure that the data are comparable across subjects, thus minimizing potential biases caused by inconsistencies in the imaging data.

**2. Slice Timing Correction**

The Slice Timing Correction tool is used to correct for acquisition time differences within the same brain scan. This step ensures that the functional data from different slices are synchronized, which is important for maintaining the temporal accuracy of the brain activity measurements.

**3. Realignment**

The Realign utility corrects for patient movement during the scanning process. This step helps eliminate motion artifacts that could distort the data, thereby enhancing the quality and reliability of the images for subsequent analysis.

**4. Co-registration**

The Co-register utility aligns the functional image with the anatomical image (mean realigned image). This ensures that functional data are mapped onto the structural brain images accurately, facilitating precise localization of brain activity. Co-registration is necessary for comparing brain regions in a consistent anatomical space.

**5. Segmentation**

The Segment utility is applied to segment various tissue structures (such as gray matter, white matter, and CSF) from the obtained co-registered image. Segmentation is a critical step that helps isolate specific brain regions for further analysis, improving the accuracy of functional data interpretation.

**6. Normalization**

The Normalize utility [22] transforms the images into a standard brain template. This step ensures that images from different subjects are aligned in a common space, eliminating anatomical variations. Normalization is essential for comparing the data across subjects in a group study.

**7. Smoothing**

The Smooth utility is used to smooth the time series of each voxel [22]. This process helps reduce noise and improve the signal-to-noise ratio, making the functional activity more detectable and reliable.

**8. Feature Extraction (ALFF, fALFF, ReHo)**

ALFF, fALFF, and ReHo feature images are calculated from the preprocessed images using the REST toolbox. These features capture key brain activity characteristics, such as low-frequency oscillations and regional synchronization, which are important for differentiating PD patients from healthy controls.

**9. Co-registration to AAL Brain Atlas**

The feature images are co-registered to the AAL brain Atlas to ensure that the extracted ROIs correspond appropriately to the regions of interest (ROIs) [23], defined in the anatomical space. This step guarantees meaningful comparisons across subjects and allows for accurate identification of specific brain regions associated with PD.

**10. Gabor Filtering**

The ROIs in the cerebellum are filtered using 18 Gabor filters. This step enhances the texture of the image by applying a set of frequency- and orientation-sensitive filters. The use of Gabor filtering helps identify spatial features related to brain activity, which can be crucial for distinguishing between PD patients and healthy controls. The images are normalized within the range of -1 to 1 for consistency.

**11. Thresholding**

The filtered images are thresholded to isolate the most

significant brain regions and remove irrelevant or noisy data. The thresholding step ensures that only the most informative features are retained for further analysis, allowing the model to focus on key patterns associated with PD.

**12. Shape-Based Parameter Calculation**

Shape-based parameters, such as perimeter, equivalent diameter, area, minor axis length, major axis length, eccentricity, and orientation, are calculated using MATLAB functions. These parameters provide quantitative measurements of the shape and size of brain structures, which are essential for distinguishing between PD patients and healthy controls.

**13. Wavelet Filtering**

The ROIs are filtered using wavelet functions in MATLAB. This step allows for the analysis of the signal across different frequency bands, enhancing the feature extraction process by highlighting important frequency components related to PD. The images are normalized within the range of -1 to 1, and thresholding is applied to the filtered images.

**14. Reclassification Using New Set of Parameters**

The shape-based parameters calculated in step 12 are reclassified using the same Decision Table and Decision Stump classifiers as in step 6. The process is repeated for the new set of parameters to evaluate the performance of the classification model with the wavelet-enhanced features.

**15. Comparison of Results**

The results from steps 13 and 14 are compared to assess the effectiveness of wavelet filtering in improving the classification accuracy between PD patients and healthy controls.

## 3. RESULTS AND DISCUSSION

The fMRI data of 10 PD patients (five men, five women, age range: 41-71) and 10 normal persons (six men, four women, age range: 45-74) was processed and then the features namely ALFF, fALFF, ReHo and functional connectivity were extracted from the processed images. 18 regions of interest (ROI's) were analyzed in the feature images using two procedures. In the first procedure, Gabor filter was used to the ROI images and the filtered images were being threshold subsequently. In the second procedure, the ROI images were decomposed by 'HAAR' wavelet, then reconstructed by level 3 coefficients and finally thresholder.

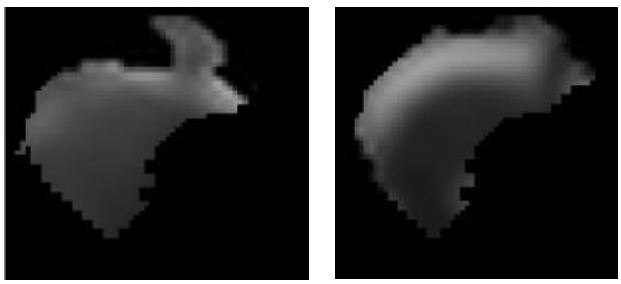

(a) (b)

**Figure 4.** Sample cross-section of ROI "Left crus I of cerebellar hemisphere" (AAL label-91) (a) ROI extracted from a healthy person's ALFF feature image (b) ROI extracted from a PD patient's ALFF feature image

The normal person's group in the selected ROI's as in Figure 4. Formidable differences in shape of regions after thresholding can be seen in Figure 5 and Figure 6, pointing to varying levels of activity between the PD patients' group. The calculation of shape parameters is the approach employed to capture the shape approximation.

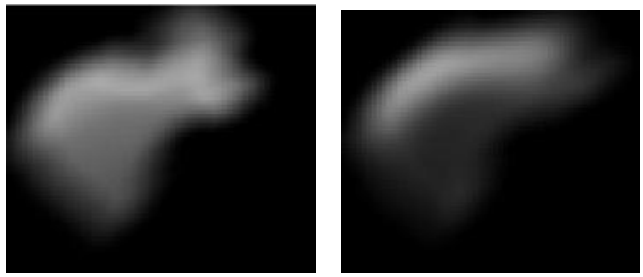

(a) (b)

**Figure 5.** A sample cross-section of ROI "Left crus I of cerebellar hemisphere" after applying Gabor filter (orientation=3*pi/4, wavelength=20) (a) Image after the application to Gabor filter (a), (b) Image after Gabor filter applied to image (b)

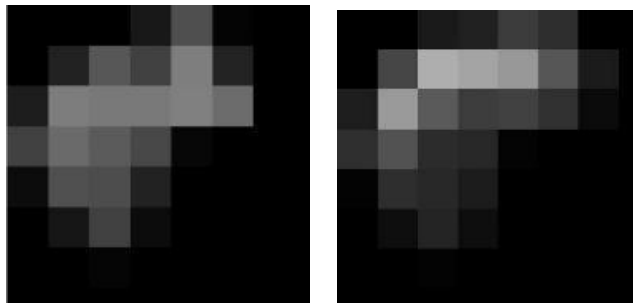

(a) (b)

**Figure 6.** A sample cross-section of ROI "Left crus I of cerebellar hemisphere" after reconstruction from level 3 approximate (a) Image after reconstruction of image (a) (b) Image after reconstruction of image (b)

The confusion matrices for best performing classifier under respective parameter extraction procedure are shown in Tables 1 and 2. The results are mentioned in Table 3. In the tables, "normal" label is used for a healthy person while the "subject" label is used for Parkinson's disease patients. Table 4 shows the performance measure parameters

**Table 1.** Confusion matrix found for parameters extracted from Gabor filtered images when classified using SMO (Sensitivity=80%)

| | | **Actual** | |
|---|---|---|---|
| | | Normal | subject |
| **Predicted** | Normal | TN=8 | FP=2 |
| | Subject | FN=2 | TP=8 |

**Table 2.** Confusion matrix for parameters extracted from wavelet analysed images when classified using Decision stump (Sensitivity=100%)

| | | **Actual** | |
|---|---|---|---|
| | | Normal | subject |
| **Predicted** | Normal | TN=8 | FP=2 |
| | Subject | FN=0 | TP=10 |

**Table 3.** Accuracy (in percentage) of the achieved by the classifiers corresponding to procedure of extracting parameters

| | Classifiers (%) | | | |
|---|---|---|---|---|
| **Methods** | **Naïve Based** | **Logistic Regression** | **SMO** | **Decision Stump** |
| Gabor Filtering | 65 | 70 | 80 | 60 |
| Wavelet Filtering | 70 | 75 | 80 | 90 |

**Table 4.** Performance measure parameters

| | **Precision** | **Recall** | **F1-Score** |
|---|---|---|---|
| Gabor Filtering | 0.8 | 0.8 | 0.8 |
| Wavelet Analysis | 0.83 | 1 | 0.90 |

The images resulting from the analysis provide favorable repercussions upon observation. Figure 4 shows samples of extracted ROI "Left crus I of cerebellar hemisphere" from ALFF feature images of a healthy person Figure 4(a) and of a PD patient Figure 4(b). On visual inspection, it can observe slight differences between the two images. As shown in Figure 5(a) and Figure 5(b), after filtering with a Gabor filter, the images are smoothed and filtered for noise. After threshold is applied to the filtered images, the regions are analyzed by 7 shape-based parameters using different machine learning methods. The same procedure is followed for other 10 healthy individuals' and 10 PD patients over the four feature categories.

Similarly, as demonstrated in Figures 6(a) and 6(b), the wavelet analysis yields observable differences in regions after images in Figure 4 decomposed to 3 levels by HAAR wavelet.

In this study, the SMO and Decision Stump classifiers were evaluated using Gabor filtering and wavelet filtering. The SMO classifier achieved an 80% sensitivity with Gabor-filtered images, while the Decision Stump classifier achieved 100% sensitivity with wavelet-processed images. The performance difference is due to the classifiers' mechanisms: SMO, an SVM-based method, excels at handling complex patterns, while Decision Stump, a simpler decision tree model, benefits from clearer segmentation provided by wavelet analysis. Clinically, the 100% sensitivity of Decision Stump with wavelet analysis highlights its potential for accurate Parkinson's disease (PD) diagnosis. Wavelet analysis enhances feature differentiation, leading to better classifier performance compared to Gabor filtering.

In comparison to existing studies, our research introduces wavelet analysis and Gabor filtering as advanced methods for extracting distinct features from brain activity. Unlike traditional methods like resting-state functional connectivity or ReHo, which use basic classifiers, our study achieves a higher classification accuracy (90% vs. 65%) with wavelet analysis and Decision Stump, showcasing improved performance over existing fMRI-based PD diagnosis approaches. The innovation lies in the ability of these techniques to capture complex, multiscale brain activity patterns, offering potential advantages for early PD diagnosis, where detecting subtle changes in brain function is critical.

## 4. CONCLUSION

This study compared the effectiveness of wavelet analysis and Gabor filtering in classifying functional brain images for Parkinson's disease diagnosis, using four classifiers: Naïve Bayes, Logistic Regression, SMO, and Decision Stump. Wavelet analysis outperformed Gabor filtering, with the Decision Stump classifier showing the greatest difference (90% vs. 65%). The Decision Stump classifier demonstrated fast training and prediction times, handling both categorical and numerical features, and can be used as a weak learner in ensemble methods like AdaBoost. The higher performance with wavelet analysis, especially the 90% sensitivity with Decision Stump, indicates its better ability to differentiate features, enhancing clinical relevance. Naïve Bayes and Logistic Regression showed improved accuracy with wavelet analysis, while SMO achieved consistent performance (80%) across both methods, highlighting its robustness.

Clinically, these results emphasize the importance of selecting the appropriate feature extraction method and classifier for reliable Parkinson's disease diagnosis, critical for early detection and treatment. However, the study has limitations, such as a small sample size (10 PD patients and 10 healthy individuals), which may affect generalizability, and testing only four classifiers. Future research should use larger datasets and explore advanced machine learning models, such as deep learning, for better classification accuracy. Additionally, integrating more feature extraction techniques could improve analysis.

The research findings hold strong clinical potential, particularly for early and differential diagnosis of Parkinson's disease. Wavelet analysis and Gabor filtering, as non-invasive, cost-effective tools, could aid in detecting early-stage Parkinson's disease, enabling timely intervention and personalized treatment strategies.

## REFERENCES


[1] Dehsarvi, A., Smith, S.L. (2019). Classification of resting-state fMRI using evolutionary algorithms: Towards a brain imaging biomarker for Parkinson's disease. arXiv preprint arXiv:1910.05378. https://doi.org/10.48550/arXiv.1910.05378

[2] Sherer, T.B., Chowdhury, S., Peabody, K., Brooks, D.W. (2012). Overcoming obstacles in Parkinson's disease. Movement Disorders, 27(13): 1606-1611. https://doi.org/10.1002/mds.25260

[3] Haq, N.F., Cai, J., Yu, T., McKeown, M.J., Wang, Z.J. (2020). Parkinson's disease detection from fMRI-derived brainstem regional functional connectivity networks. In Medical Image Computing and Computer Assisted Intervention–MICCAI 2020: 23rd International Conference, Lima, Peru, pp. 33-43. https://doi.org/10.1007/978-3-030-59728-3_4

[4] Prashanth, R., Roy, S.D., Mandal, P.K., Ghosh, S. (2014). Automatic classification and prediction models for early Parkinson's disease diagnosis from SPECT imaging. Expert Systems with Applications, 41(7): 3333-3342. https://doi.org/10.1016/j.eswa.2013.11.031

[5] Baudrexel, S., Witte, T., Seifried, C., von Wegner, F., Beissner, F., Klein, J.C., Hilker, R. (2011). Resting state fMRI reveals increased subthalamic nucleus–motor cortex connectivity in Parkinson's disease. Neuroimage, 55(4): 1728-1738. https://doi.org/10.1016/j.neuroimage.2011.01.017

[6] Luo, C., Chen, Q., Song, W., Chen, K., Guo, X., Yang,

J., Shang, H.F. (2014). Resting-state fMRI study on drug-naive patients with Parkinson's disease and with depression. Journal of Neurology, Neurosurgery & Psychiatry, 85(6): 675-683. https://doi.org/10.1136/jnnp-2013-306237

[7] Desco, M., Hernandez, J.A., Santos, A., Brammer, M. (2001). Multiresolution analysis in fMRI: Sensitivity and specificity in the detection of brain activation. Human Brain Mapping, 14(1): 16-27. https://doi.org/10.1002/hbm.1038

[8] Faragó, P., Tuka, B., Tóth, E., Szabó, N., Király, A., Csete, G., Kincses, Z.T. (2017). Interictal brain activity differs in migraine with and without aura: Resting state fMRI study. The Journal of Headache and Pain, 18: 8. https://doi.org/10.1186/s10194-016-0716-8

[9] Xu, T., Cullen, K. R., Mueller, B., Schreiner, M.W., Lim, K.O., Schulz, S.C., Parhi, K.K. (2016). Network analysis of functional brain connectivity in borderline personality disorder using resting-state fMRI. NeuroImage: Clinical, 11: 302-315. https://doi.org/10.1016/j.nicl.2016.02.006

[10] Ji, G.J., Hu, P., Liu, T.T., Li, Y., Chen, X., Zhu, C., Wang, K. (2018). Functional connectivity of the corticobasal ganglia-thalamocortical network in Parkinson disease: A systematic review and meta-analysis with cross-validation. Radiology, 287(3): 973-982. https://doi.org/10.1148/radiol.2018172183

[11] Brumm, M.C., Siderowf, A., Simuni, T., Burghardt, E., Choi, S.H., Caspell-Garcia, C., et al. (2023). Parkinson's progression markers initiative: A milestone-based strategy to monitor Parkinson's disease progression. Journal of Parkinson's Disease, 13(6): 899-916. https://doi.org/10.3233/JPD-223433

[12] Zou, Q.H., Zhu, C.Z., Yang, Y., Zuo, X.N., Long, X.Y., Cao, Q.J., Zang, Y.F. (2008). An improved approach to detection of amplitude of low-frequency fluctuation (ALFF) for resting-state fMRI: Fractional ALFF. Journal of Neuroscience Methods, 172(1): 137-141. https://doi.org/10.1016/j.jneumeth.2008.04.012

[13] Zang, Y., Jiang, T., Lu, Y., He, Y., Tian, L. (2004). Regional homogeneity approach to fMRI data analysis. Neuroimage, 22(1): 394-400. https://doi.org/10.1016/j.neuroimage.2003.12.030

[14] Brett, M. (2011). MarsBaR Documentation. Functional Imaging, pp. 1-45.

[15] Prashanthi, G., Singh, S., Rajan, E.G., Krishnan, P. (2014). Sparsification of voice data using Discrete Rajan Transform and its applications in speaker recognition. In 2014 IEEE International Conference on Systems, Man, and Cybernetics (SMC), San Diego, CA, USA, pp. 429-434. https://doi.org/10.1109/SMC.2014.6973945

[16] Olowoyeye, A., Tuceryan, M., Fang, S. (2009). Medical volume segmentation using bank of Gabor filters. In Proceedings of the 2009 ACM Symposium on Applied Computing, pp. 826-829. https://doi.org/10.1145/1529282.1529458

[17] Shulman, R.G., Rothman, D.L., Behar, K.L., Hyder, F. (2004). Energetic basis of brain activity: Implications for neuroimaging. Trends in Neurosciences, 27(8): 489-495. https://doi.org/10.1016/j.tins.2004.06.005

[18] Nikolaou, F., Orphanidou, C., Papakyriakou, P., Murphy, K., Wise, R.G., Mitsis, G.D. (2016). Spontaneous physiological variability modulates dynamic functional connectivity in resting-state functional magnetic resonance imaging. Philosophical Transactions of the Royal Society A: Mathematical, Physical and Engineering Sciences, 374(2067): 20150183. https://doi.org/10.1098/rsta.2015.0183

[19] Jacobs, C.E., Finkelstein, A., Salesin, D.H. (1995). Fast multiresolution image querying. In Proceedings of the 22nd Annual Conference on Computer Graphics and Interactive Techniques, pp. 277-286. https://doi.org/10.1145/218380.218454

[20] Duchesne, S., Rolland, Y., Vérin, M. (2009). Automated computer differential classification in Parkinsonian syndromes via pattern analysis on MRI. Academic Radiology, 16(1): 61-70. https://doi.org/10.1016/j.acra.2008.05.024

[21] Salvatore, C., Cerasa, A., Castiglioni, I., Gallivanone, F., Augimeri, A., Lopez, M., Quattrone, A. (2014). Machine learning on brain MRI data for differential diagnosis of Parkinson's disease and Progressive Supranuclear Palsy. Journal of Neuroscience Methods, 222: 230-237. https://doi.org/10.1016/j.jneumeth.2013.11.016

[22] Ashburner, J., Barnes, G., Chen, C., Daunizeau, J., Flandin, G., Friston, K., Phillips, C. (2012). SPM8 manual. Functional Imaging Laboratory, Institute of Neurology, 41.

[23] Song, X.W., Dong, Z.Y., Long, X.Y., Li, S.F., Zuo, X.N., Zhu, C.Z., Zang, Y.F. (2011). REST: A toolkit for resting-state functional magnetic resonance imaging data processing. PloS One, 6(9): e25031. https://doi.org/10.1371/journal.pone.0025031